RESEARCH LETTER

Structure–activity analysis suggests an olfactory function for the unique antennal delta glutathione transferase of *Apis mellifera*

Mathieu Schwartz[1] , Valentin Boichot[1], Mariam Muradova[1,2], Pablo Fournier[3], Patrick Senet[4], Adrien Nicolai[4], Francis Canon[1], Frederic Lirussi[5], Ruben Ladeira[5], Martine Maibeche[6], Thomas Chertemps[6], Emmanuel Aubert[7], Claude Didierjean[7] and Fabrice Neiers[1]

1 CSGA, Flavour Perception: Molecular Mechanisms (Flavours), Université de Bourgogne, INRAE, CNRS, Institut Agro, Dijon, France
2 International Research Center "Biotechnologies of the Third Millennium", Faculty of Biotechnologies (BioTech), ITMO University, Saint-Petersburg, Russia
3 Independent Researcher, Charlotte, NC, USA
4 Laboratoire Interdisciplinaire Carnot de Bourgogne, UMR 6303 CNRS, Université de Bourgogne Franche-Comté, Dijon, France
5 Plateforme PACE, Laboratoire de Pharmacologie-Toxicologie, Bioinformatique & Big Data Au Service de La Santé 2B2S, UFR Santé, Université de Franche-Comté, INSERM U1231, Centre Hospitalier Universitaire, Besançon, France
6 Institut d'Ecologie et des Sciences de l'Environnement de Paris, Sorbonne Université, INRAE, CNRS, IRD, UPEC, Paris, France
7 Université de Lorraine, CNRS, CRM2, Nancy, France

Glutathione transferases (GST) are detoxification enzymes that conjugate glutathione to a wide array of molecules. In the honey bee *Apis mellifera*, AmGSTD1 is the sole member of the delta class of GSTs, with expression in antennae. Here, we structurally and biochemically characterized AmGSTD1 to elucidate its function. We showed that AmGSTD1 can efficiently catalyse the glutathione conjugation of classical GST substrates. Additionally, AmGSTD1 exhibits binding properties with a range of odorant compounds. AmGSTD1 has a peculiar interface with a structural motif we propose to call 'sulfur sandwich'. This motif consists of a cysteine disulfide bridge sandwiched between the sulfur atoms of two methionine residues and is stabilized by CH...S hydrogen bonds and S...S sigma-hole interactions. Thermal stability studies confirmed that this motif is important for AmGSTD1 stability and, thus, could facilitate its functions in olfaction.

Keywords: antennae; *Apis mellifera* GSTD1; glutathione transferase; odorant; stability; sulfur sandwich

Honey bees, notably *Apis mellifera*, hold significant ecological and economic importance due to their pivotal roles in pollinating crops, flowers and fruit trees [1]. Over the past decade, global declines in bee and pollinator populations have been observed, resulting from a confluence of multiple stressors encompassing biological, environmental and chemical factors [2]. This decline provides a pressing impetus to investigate and comprehend the interactions between honey bees and their environment.

In the realm of highly social insects such as honey bees, chemical communication assumes a vital role in

Abbreviations
AmGSTD1, *Apis mellifera* GST Delta 1; AmGSTD1C127S, *Apis mellifera* GST Delta 1 in which the cysteine at position 127 was changed to a serine; AmGSTD1M126L, *Drosophila melanogaster* GST Delta 1 in which the methionine at position 126 was changed to a leucine; CD, circular dichroism; CDNB, 1-chloro-2,4-dinitrobenzene; DTT, dithiothreitol; GSH, glutathione; GST, glutathione transferase; ITC, isothiocyanate.

activities such as colony maintenance, developmental processes, regulation of behaviour, caste transitions and defensive behaviours [3]. This mode of communication hinges on distinct anatomical systems responsible for sensing volatile and nonvolatile chemicals—namely the olfactory and gustatory systems. Antennae, the principal olfactory organ of insects, consist of three main segments: the scape, pedicels and flagellum. These segments, particularly the flagellum in hymenopterans, are adorned with hair-like sensilla within which receptors, such as odorant receptors, detect a wide array of sensory modalities, including odours, CO_2 and water. Chemical detection in insects entails membrane receptors situated on receptor neurons, supported by a diverse range of proteins. These proteins, including enzymes involved in metabolizing odorant molecules and odorant-binding proteins, are pivotal for transportation, safeguarding against odorant toxicity and modulating perception [4]. Prominent enzyme superfamilies characterized in the insect antennae comprise cytochrome P450 monooxygenases, glutathione transferases (GSTs), UDP-glycosyltransferase and carboxylesterases, which could help to protect these sensitive organs where neurons are directly exposed to xenobiotics, while other players, such as glutathione peroxidases, contribute to oxidative stress resistance [5–7].

Glutathione transferases (EC 2.5.1.18) are part of a ubiquitous protein superfamily present across all cellular organisms, including bacteria, plants, insects and humans [8]. Based on structural similarities and the genes encoding them, insect GSTs are categorized [9] into six canonical classes: Delta, Epsilon, Omega, Sigma, Theta and Zeta [10]. Delta is observed widely in arthropods [11], and Epsilon is probably exclusive to insects [10]. These enzymes are involved in various biological functions, through a range of GST activities, encompassing the covalent conjugation of glutathione (GSH) to hydrophobic compounds with electrophilic centres, rendering products more water-soluble [12]. Additionally, GSTs participate in noncovalent ligand binding, peroxide deactivation, catalytic isomerization and ester hydrolysis, among other processes [13–15]. For instance, DmGSTE14, discovered in Drosophila, plays a pivotal role in hormone production *via* isomerization, and its absence results in larval developmental arrest [15–17].

Glutathione transferases were shown to be expressed in the antennae of various orders of insect species [4], such as the dipteran *Drosophila melanogaster* [18,19], as well as in antennaed lepidopteran species [20–28] or coleopteran antennae [29,30]. Insect antennae GSTs serve dual roles in both safeguarding chemosensory organs [31–34] and influencing compound detection in

insects [26,28,35–37]. Structural studies have been carried out on members of the two main classes of GSTs in insects, the epsilon and delta classes. They exhibit the canonical GST dimer with the active site harbouring the glutathione binding site hosted by the thioredoxin N-terminal domain and the hydrophobic binding site located on the helical C-terminal domain. Additionally, specific features distinguish the delta from the epsilon in the dimer interface, namely a clasp motif in the delta [38] and a wafer motif in the epsilon [39].

In *A. mellifera*, 10 functional GST-encoding genes have been identified, a significantly smaller number than the 38 GST-encoding genes found in *D. melanogaster* (fruit fly) and the 31 genes in *Anopheles gambiae* (mosquito). Focusing on insect-specific GST classes, *A. mellifera* lacks any epsilon class enzymes and retains only one member of the delta class (AmGSTD1), in contrast to the 11 delta and 14 epsilon class members in *D. melanogaster* and 12 delta and 8 epsilon class members in *A. gambiae* [4,40]. Notably, the AmGSTD1 is prominently expressed in the antennae of drones, workers and queens [5,41]. It has been suggested that honey bees' foraging and feeding behaviours, as well as their eusocial organization, are responsible for the low amounts of detoxifying genes in the genome. Bees and plants share a mutualistic interaction, in which plants provide nectar and pollen while receiving the benefit of the pollination activities of honey bees. However, honey bees are not physiologically adapted to the constant exposure to chemicals produced by plants and humans. This attribute, however, renders honey bees especially sensitive to certain insecticides [42].

To elucidate the function of honey bee GSTD1 (AmGSTD1), we undertook its production, purification and biochemical and structural analysis. Concurrently, we explored the enzymatic capacity towards classical substrates as well as its capacity to interact with odorants in the context of antennal expression. An original dimerization interface was discovered, which has evolved to enhance the stability supported by the biochemical and structural analysis of two proteinic variants at the positions involved in interface stabilization.

Materials and methods

Cloning, expression and purification of wild-type AmGSTD1, AmGSTD1^{M126L} and AmGSTD1^{C127S} enzymes

The DNA encoding the wild-type protein sequence of *A. mellifera* GSTD1 (NP_A0A7M7GUY7) was subjected to codon optimization for expression in *Escherichia coli*.

Codons corresponding to the initial 26 amino acids, which extended beyond the conventional insect GST sequences and potentially indicated a signal peptide, were excised. The DNA sequences encoding the AmGSTD1^{M126L} and AmGSTD1^{C127S} enzyme variants were generated through substitution of the codon corresponding to a methionine at position 126 with a codon encoding a leucine and the codon corresponding to a cysteine at position 127 with a serine. The synthesized DNA sequences were procured from Genewiz (Leipzig, Germany) and subsequently sub-cloned and inserted into the pET22b vector (Novagen, Darmstadt, Germany) *via* the *NdeI* and *SacI* restriction sites. The resulting plasmids were utilized for transforming the *E. coli* BL21 star strain. Colonies isolated from an LB-ampicillin agar plate (50 mg·L^{-1} ampicillin) were employed to inoculate a 50 mL LB-ampicillin culture (50 mg·L^{-1} ampicillin), which was then cultivated overnight at 37 °C.

Subsequently, the 50 mL culture served to inoculate a larger 4 L LB-ampicillin medium. Protein expression was induced at an OD$_{600nm}$ of 0.6 through the addition of 1 mM (final concentration) isopropyl β-D-1-thiogalactopyranoside, followed by continued bacterial growth for 18 h at 37 °C. The resultant cells were harvested through centrifugation (4000 *g*, 20 min, 4 °C), resuspended in binding buffer (20 mM sodium phosphate, 0.5 M NaCl, 100 μM DTT and 20 mM imidazole, pH 7.4) and subjected to sonication (Vibracell; Bioblock, Pittsburgh, PA, USA) at 4 °C for disruption. Following centrifugation at 20 000 *g* for 45 min at 4 °C, the supernatant was loaded onto a GSTrap HP 5 mL column (Cytiva, Washington, DC, USA). The column was washed with PBS buffer, pH 7.0 and GST was eluted utilizing a 50 mM Tris–HCl buffer, pH 7.4, supplemented with 10 mM reduced GSH. Fractions containing GST were pooled, dialysed against 100 mM potassium phosphate buffer at pH 6.5 and concentrated to 10 mg·mL^{-1} using an Amicon Ultra spin column with a molecular weight cut-off of 10 kDa (Millipore, Billerica, MA, USA). Protein purity higher than 99% was confirmed *via* Coomassie-stained 15% SDS/PAGE gel analysis. The wild-type and variant AmGSTD1 were dialysed against 100 mM sodium phosphate buffer, pH 6.5 before kinetic measurements and far-UV circular dichroism.

Kinetic measurements

CDNB, GSH, isothiocyanates (ITCs) and odorants were purchased from Merck (Kenilworth, NJ, USA). All substrates except GSH were dissolved in ethanol or methanol. The final solvent concentration in the reaction system was kept at a maximum of 5% (v/v).

Specific activities were determined spectrophotometrically at 20 °C using 1 mM GSH, a variable concentration of substrate and a concentration of enzyme adapted from the enzymatic rate. A 100 mM sodium phosphate buffer, pH 6.5, was used for all assays. The K_M for GSH was measured with a variable concentration of GSH and a 1 mM concentration of CDNB. CDNB glutathionylation was monitored at 340 nm (with an extinction coefficient, ε, of 9.6 mM^{-1}·cm^{-1}). Similarly, GSH-conjugated ITCs were monitored at 274 nm for allyl-ITC (ε = 7.45 mM^{-1}·cm^{-1}); benzyl-ITC at 274 nm (ε = 9.25 mM^{-1}·cm^{-1}); butyl-ITC at 274 nm (ε = 7.75 mM^{-1}·cm^{-1}); hexyl-ITC at 274 nm (ε = 6.55 mM^{-1}·cm^{-1}); phenethyl-ITC at 274 nm (ε = 8.89 mM^{-1}·cm^{-1}); and propyl-ITC at 274 nm (ε = 8.35 mM^{-1}·cm^{-1}).

Steady-state kinetic parameters were determined under the respective assay conditions, utilizing varying substrate concentrations. Nonlinear regression was employed to fit the Michaelis–Menten and Hill equations to the data, yielding values for K_M, V_{max} and the Hill coefficient. V_{max} values were subsequently converted into k_{cat} values based on the molar concentration of the enzyme.

To measure the ability of AmGSTD1 to interact with odorant molecules, we used a previously published method [35,43,44]. The CDNB enzyme-based competition assay allows us to identify compounds that are conjugated or bind the enzyme without conjugation (ligandin function) to decrease enzymatic activity towards CDNB. CDNB conjugation was measured at 20 °C using 1 mM GSH and CDNB, 10 nM AmGSTD1 and two concentrations (10 and 100 μM) of the tested odorant in 100 mM sodium phosphate buffer, pH 6.5. The slope of the initial rate of the reaction was measured in triplicate and compared with the slope obtained in the same conditions but supplemented with a 10 or 100 μM concentration of the tested molecule. Stock solutions of molecules were prepared in methanol at a concentration of 100 mM. All solutions were aggregate-free and stored at −20 °C. The inhibition percentage was calculated using a previous method [35,43,44], and the values presented are the mean of three independent measurements with standard deviations.

Far-UV circular dichroism

Far-UV circular dichroism (CD) spectra were recorded using a JASCO J-815 spectropolarimeter (Tokyo, Japan) equipped with Peltier temperature control. The proteins were prepared at a concentration of 2.5 μg·mL^{-1} in 0.01 M phosphate buffer at pH 6.5. Using a 1-cm path-length quartz cell, the protein sample spectra were recorded with a scan speed of 50 nm·min^{-1} between 200 and 240 nm. Spectra were averaged over three scans. For each enzyme, the spectra were consistently recorded within the same quartz cell while systematically increasing the temperature in 1 °C intervals from 30 °C to 80 °C. The values obtained at 220 nm were plotted as a function of the temperature for each enzyme. The thermal denaturation data were processed using CDPAL software (version 2.18) [45]. Data were normalized and fitted to the two-state model using the standard *Autofit* procedure, which allowed us to calculate the

Crystallization and diffraction data collection of wild-type AmGSTD1, AmGSTD1^{M126L} and AmGSTD1^{C127S}

Before crystallization assays, the wild-type and variant AmGSTD1 were dialysed against 20 mM pH 8.0 Tris–HCl and concentrated to 15 mg·mL^{-1}. Crystallization trials were performed manually at 20 °C. Wild-type AmGSTD1 was crystallized in microbatches under oil by mixing 1 μL of protein with 1 μL of solution containing 16% (w/v) PEG4000, 10% (w/v) 2-propanol, 0.1 M HEPES pH 7.5 and 0.2 M ammonium sulfate. The drops were covered with 30 μL of paraffin oil (CAS n°8042-47-5; Merck). The variant AmGSTD1^{M126L} was crystallized in sitting drop by mixing 1 μL of protein with 1 μL of solution containing 15% (w/v) PEG4000, 0.1 M trisodium citrate pH 5.6 and 0.2 M ammonium sulfate in a drop equilibrated against a reservoir filled with 100 μL of the same solution. The variant AmGSTD1^{C127S} was crystallized in sitting drop by mixing 1 μL of protein with 1 μL of solution containing 22% (w/v) PEG4000, 0.1 M sodium acetate and 0.2 M ammonium sulfate in a drop equilibrated against a reservoir filled with 100 μL of the same solution. All crystals appeared within a few days. Crystals were cryoprotected with 20% (w/v) glycerol and flash-frozen in liquid nitrogen before synchrotron data collection. Diffraction experiments were performed on the beamline FIP2 of synchrotron ESRF and on the beamline PROXMA1 of the synchrotron SOLEIL (Saint-Aubin, France). Wild-type AmGSTD1 crystals, AmGSTD1^{M126L} crystals and AmGSTD1^{C127S} crystals diffracted to 2.05, 1.75 and 1.50 Å, respectively. The datasets were indexed and integrated with XDS [46] and scaled with AIMLESS [47]. The structure of AmGSTD1 was solved by molecular replacement using the coordinates of *Nilaparvata lugens* GST Delta (PDB code 3WYW) [48] as a model in BALBES [49]. The 3D structure was built graphically with COOT [50] and refined with PHENIX [51]. Validation was carried out with MOLPROBITY [52]. Figures were prepared using PYMOL (The PyMOL Molecular Graphics System, Version 2.0; Schrödinger, LLC, New York, NY, USA). Coordinates and structure factors of AmGSTD1,

AmGSTD1^{M126L} and AmGSTD1^{C127S} have been deposited in the Protein Data Bank under accession codes 8Q89, 8Q8A and 8Q8B, respectively. Data and refinement statistics are summarized in Table S1.

DFT calculations

DFT calculations (B3LYP-D3/Def2TZVPP) were performed on a model of the dimer (Met-Cys)$_2$ (Fig. S1) using GAUSSIAN16 software (Pittsburgh, PA, USA); hydrogen atoms were optimized while the heavy atoms were maintained at the experimental XRD geometry. Interatomic interactions were characterized through NCI analysis [53] using MWFN software [54]; calculation results are depicted in Fig. S1. Previous studies have shown that these calculation conditions are suitable for characterizing sigma-hole interactions involving chalcogen and halogen atoms [55].

Results and Discussion

Wild-type AmGSTD1 enzymatic activities

AmGSTD1 wild-type was obtained in pure form following one step of affinity chromatography. To assess general enzymatic competence, we conducted experiments with well-known GST substrates, encompassing 1-chloro-2,4-dinitrobenzene (CDNB) and seven commercially available isothiocyanates (ITCs), as detailed in Table 1. Notably, AmGSTD1 exhibited elevated k_{cat} value alongside low K_M value for CDNB. The higher K_M value for GSH, 732 μM, could account for a potential underestimation of the k_{cat} value measured for CDNB, which is expected to be equivalent. Due to a strong increase in the nonenzymatic reaction, the possibility of working with a higher value of GSH is limited. Despite this limitation, the observed efficiency (k_{cat}/K_M) towards CDNB, at 320 s^{-1}·mM^{-1}, already surpasses the efficiency values previously documented for *D. melanogaster* Delta GSTs [56]. The efficiency of AmGSTD1 closely approaches that of 281 s^{-1}·mM^{-1} measured for *D. melanogaster* GSTD11, the most efficient *D. melanogaster* Delta GST. Interestingly, GSTD11 appears to be the most probable orthologue

Table 1. Steady-state parameters of wild-type AmGSTD1 for CDNB, GSH and different selected ITCs. K_M and k_{cat} values were calculated by nonlinear regression based on the Michaelis–Menten model and Hill equation. The Michaelis–Menten model was applicable for all the tested substrates except phenethyl-ITC. The K_M value for GSH was determined using 1 mM CDNB substrate. The values for the electrophilic substrates were similarly obtained with a 1 mM concentration of GSH. N.A., not applicable.

	CDNB	GSH	Allyl-ITC	Propyl-ITC	Butyl-ITC	Hexyl-ITC	Benzyl-ITC	Phenethyl-ITC	Sulforaphane
k_{cat} (min^{-1})	1620 ± 60	2500 ± 220	322 ± 62	262 ± 12	168 ± 3	88 ± 8	128 ± 16	40 ± 2	188 ± 38
K_M (μM)	84 ± 14	723 ± 166	192 ± 84	183 ± 19	95 ± 7	48 ± 13	96 ± 4	17 ± 1	266 ± 108
Hill coefficient	N.A.	N.A.	N.A.	N.A.	N.A.	N.A.	N.A.	5 ± 1	N.A.

of AmGSTD1 among the 11 Delta GSTs found in *D. melanogaster*. Using a saturating concentration of CDNB, the K_M for GSH was measured in the same range as K_M values measured for Delta *D. melanogaster* GSTs. The GSH efficiency is $58 \text{ s}^{-1} \cdot \text{mM}^{-1}$ compared with $360 \text{ s}^{-1} \cdot \text{mM}^{-1}$ previously measured for the DmGSTD11 orthologous enzyme. Considering the pronounced spontaneous reactivity of ITCs with GSH, determination of the ITC K_M value is possible only when K_M towards ITCs is low, thereby allowing work with lower ITC concentrations. In the case of AmGSTD1, K_M and k_{cat} values were measured for all six tested ITCs due to low K_M towards these six molecules. AmGSTD1 is highly efficient with these six substrates. Significantly, a trend emerges as the carbon chain length increases, resulting in a concomitant decrease in the Michaelis–Menten constant (K_M). Moreover, heightened steric hindrance, which is predominantly conspicuous within aromatic ITCs, demonstrates a discernible correlation with the reduction in K_M. In contrast, this diminution in K_M, concurrent with the elongation of the carbon chain, corresponds to a commensurate decrement in the catalytic rate. The distinctive case of sulforaphane provides compelling evidence that the sulfoxide functional moiety yields an unfavourable effect, thereby counterbalancing the influence of a four-carbon chain and inducing a threefold elevation in K_M relative to the four-carbon butyl-ITC reference. Phenethyl-ITC was the only tested substrate in this study that exhibited strong positivity cooperativity, supported by a high value of the Hill coefficient (5 ± 1). A cooperativity mechanism was previously observed for other insect GSTs of the Delta family in *D. melanogaster* or *Anopheles dirus* [57,58].

Wild-type AmGSTD1 interact with odorants

AmGSTD1 was previously shown to be highly expressed in *A. mellifera* antennae, suggesting its potential role in olfaction [41]. Taking into account its efficient catalytic activity towards classical substrates, which supports the functionality of this enzyme, 27 different odorants that are mainly found in plants and/or have shown an activity involving the chemosensory system were tested at two concentrations (Fig. 1, Table S2). A low inhibitory effect was observed for most of them, corresponding to their capacity to interact with AmGSTD1. The interaction can be due to a catalytic activity towards the tested odorant as well as a binding without catalysis. These interactions are not surprising due to the large range of molecules able to interact with GSTs in a general

manner. However, only three odorants were able to inhibit AmGSTD1 at more than 30% at a concentration of 100 μM: alpha-pinene, benzaldehyde and benzyl alcohol, three biological relevant odorants for bees. Benzaldehyde, an odorant molecule detected by bee's antennae and triggering aversive behaviour, appears to be the best binder towards the tested molecules. Previously, the closest GST orthologue of AmGSTD1 in the sphinx moth *Manduca sexta* was shown to be highly expressed in the olfactory sensilla and active towards trans-2-hexenal, a plant-derived green leaf aldehyde known to stimulate the olfactory system [28]. In *Grapholita molesta*, *Plodia interpunctella* and *Sitophilus zea*mais, orthologues of AmGSTD1 were shown to metabolize alcohols, esters and aldehydes [37,59,60]. Recently, the GSTD1 from *Holotrichia parallela*, identified from the antennal transcriptome, was shown to catalyse the glutathione conjugation of various unsaturated aldehyde volatiles [61]. Altogether, this suggests a possible role of AmGSTD1 in bee olfaction acting towards various odorants.

Wild-type AmGSTD1 crystal structure analysis

We solved the crystal structure of AmGSTD1 at 2.05 Å resolution in the $P4_32_12$ space group, corresponding to one subunit in the asymmetric unit (Table S1). The crystal structure of AmGSTD1 corresponds to the typical GST fold with an N-terminal thioredoxin-like α/β domain and a C-terminal bundle of α-helices (Fig. 2A). The closest structural homologues showing an RMSD below 1.00 Å, as identified by PDBeFold [62], were the structures of GST delta proteins from *N. lugens* (PDB entry 3WYW), *A. gambiae* (PDB entry 1PN9) and GST delta 2 from *D. melanogaster* (PDB entry 5F0G).

By the time we conducted the study, a structure of GST delta from *A. mellifera* in complex with glutathione was released without publication in the PDB (PDB entry 7RHP). Monomeric superposition of our structure onto this GSH-bound form yielded an RMSD of 0.29 Å, which shows the high structural similarity between the two structures (Fig. 2A). This comparison allowed us to identify the glutathione binding site residues, as our structure lacks any ligand. The glutathione binding site residues are Glu89 and Ser90, which stabilize the gamma-glutamyl moiety; Ile77, which precedes cis-Pro78 and stabilizes the main chain of the cysteinyl moiety by its main chain; Ser34, which interacts with the cysteinyl side chain; and His75, which interacts by H-bond with the carboxy terminus of glutathione (Fig. 2B). These residues are mainly conserved in the Delta class, as mentioned
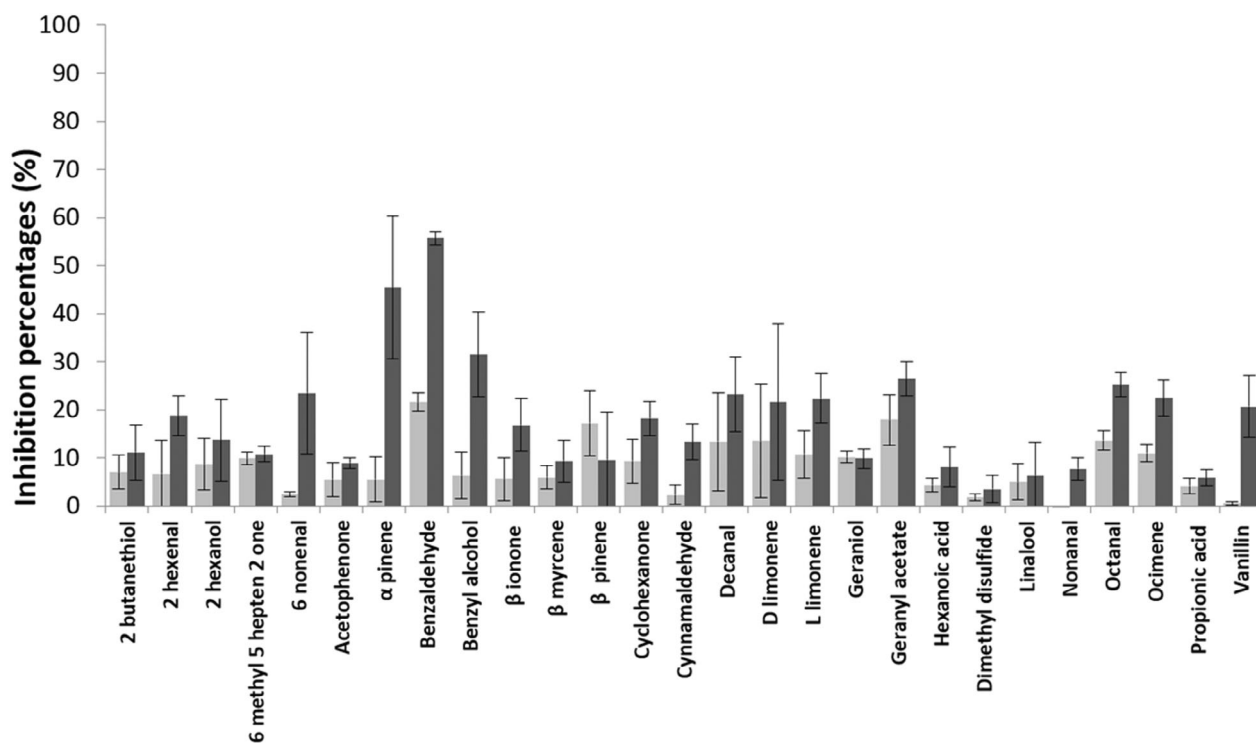
Fig. 1. Measure of the inhibition rates of odorant molecules towards wild-type AmGSTD1 activity. Inhibition of wild-type AmGSTD1 by 27 floral odorant molecules. The inhibition rates on the CDNB activity were calculated in the presence of 10 or 100 μM odorant (light and dark grey colours, respectively). The error bars show the standard deviation and were calculated from three independent experiments. The best inhibitors are indicated by the highest inhibition rate.

previously [35]. Additionally, our structure is devoid of any visible residues in the electron density map in the region between Val56 and Thr76, corresponding to the alpha 2 helix, which could be a flexible region important for glutathione binding, as previously shown through molecular dynamics simulation [35]. The absence of any ligand precluded an exact identification of the hydrophobic binding site (H site) residues. However, the superimposition of AmGSTD1 structure onto the previously solved structure of *A. dirus* GST delta 4 in complex with hexyl-glutathione allowed to identify putative H site residues (Fig. S2). This H site is in close vicinity of the G site as conserved in the GST family and is mainly constituted by aromatic residues.

The biological dimer of AmGSTD1, as predicted by the PISA server [63], can be generated by using crystallographic symmetry. An in-depth analysis of the interface of AmGSTD1 was carried out. AmGSTD1 exhibits the typical motif of Delta GSTs in its interface, namely the clasp motif (Fig. 2C). This structural feature in AmGSTD1 corresponds to the aromatic residue Tyr123 from subunit A that fits between helices alpha 3 and alpha 4 from subunit B. Both Tyr123 side

chains from subunits A and B are located around the twofold axis, making this structural motif important for the stability of the dimer [38]. Additionally, AmGSTD1 shows original features for a GST Delta, detailed in the following. Cys127 forms a disulfide bridge with the same Cys residue from its neighbouring subunit, thus constituting a covalent dimer (Fig. 2C). Additionally, in the vicinity of the Cys127-Cys127 disulfide bridge, the side chains of both Met126 residues interact with the S-S bond. This close proximity of the four sulfur atoms (from the Cys and Met residues) forms an unusual and unique structural motif that we propose to call the 'sulfur sandwich' (Fig. 2C). The distance between the sulfur atoms of Cys127 and Met126, at 2.9 Å, is significantly less than the sum of their van der Waals radii (3.6 Å). Consequently, this proximity cannot be interpreted as a van der Waals interaction. The sulfur sandwich interaction was tentatively characterized through DFT calculations on a model dimer $(Met-Cys)_2$ (Fig. S1), displaying the same structure than the motif 'Met126Cys127—Cys127Met126' in the oxidized form of AmGSTD. This analysis revealed two interactions between the Cys sulfur atom and the side chain of Met126: an
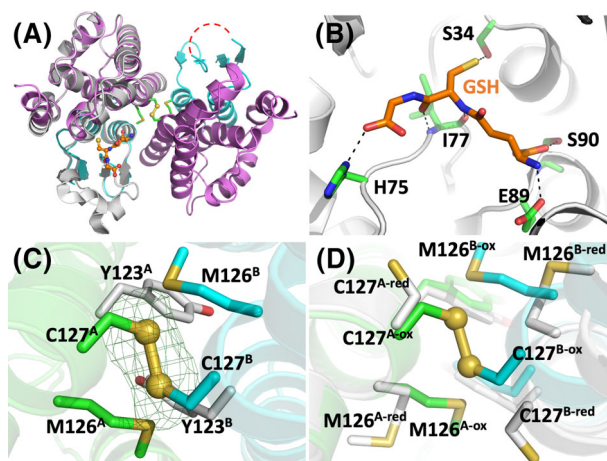
Fig. 2. Crystal structures of *Apis mellifera* GSTD1. (A) Global view of the AmGSTD1 dimer in cartoon view with the N-terminal domain coloured cyan and the C-terminal domain coloured magenta. A monomeric superimposition is shown with the GSH-bound form of AmGSTD1 (PDB 7RHP) in white. GSH is coloured orange, and the sulfur sandwich motif is coloured green. The missing helix alpha 2 in PDB 8Q89 (this study) is represented as red dashed lines. (B) Glutathione binding site as present in the structure of the GSH-bound form (PDB 7RHP). (C) Focus on the sulfur sandwich with an omit mFo-DFc map contoured at 3.0 sigma around the disulfide bridge (green and cyan) linking both monomers. The clasp motif has been coloured white. (D) Superimposition between PDB 8Q89 (disulfide-bridged form, green and cyan) and PDB 7RHP (reduced form, white) and focus on the sulfur sandwich.
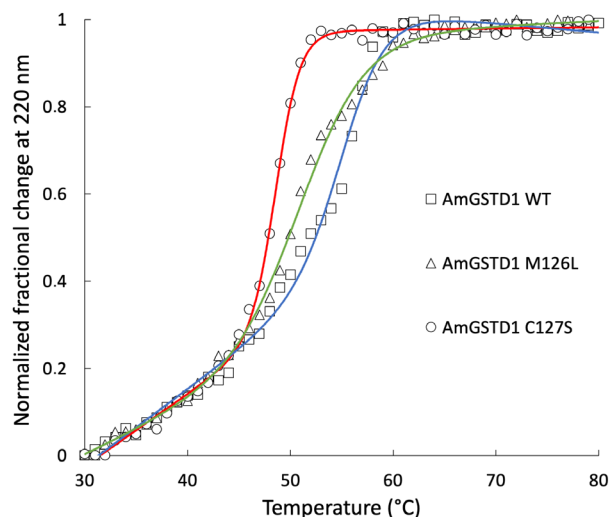

Fig. 3. Temperature denaturation of wild-type and variants AmGSTD1 followed by the normalized fractional change at 220 nm measured from CD experiments. The data were fitted with the CDPAL software and each experiment was performed in triplicate.

[126]C-H...S[127] hydrogen bond involving a methylene moiety of Met126 and an [126]S...S[127] sigma-hole interaction. Although the geometry of the latter interaction is not optimal [64], it is noteworthy as it is still relatively unexplored in the field of three-dimensional protein structures [65]. This sulfur sandwich is not present in the reduced structure (PDB 7RHP), as Cys127 is oriented towards their respective monomers (Fig. 2D). The same observation is true for the Met residues in the reduced structure (Fig. 2D). The sulfur sandwich probably forms upon cysteine oxidation and formation of the disulfide bond, with the methionine residues adding σ-hole effects and thus additional stability to the covalent link.

Crystal structures and thermal stability of the variants AmGSTD1^M126L and AmGSTD1^C127S

To test the role of the cysteine and methionine residues in the sulfur sandwich, the two variants AmGSTD1^M126L and AmGSTD1^C127S were produced and purified, and both crystal structures were solved (isomorphous to the wild-type) (Table S1).

Comparison of the structures of the mutants to the wild-type revealed no major difference (Fig. S3A,B). For AmGSTD1^C127S and the side chain of the newly introduced Ser127 points towards the monomer with the same conformation as Cys127 in the reduced structure (Fig. S3C). For AmGSTD1^M126L, the side chain of the newly introduced Leu126 maintains a conformation similar to that of Met126 in the wild-type (Fig. S3D). Both Cys127 sulfur atoms are at a distance of 2.9 Å, which could indicate a partial breaking of the disulfide bound by X-rays during diffraction experiments. To assess the contribution of the two residues M126 and C127 to the stability of the dimer, a thermal stability study using CD was carried out on wild-type AmGSTD1 and both variants (Fig. 3). The wild-type AmGSTD1 was subjected to incubation with the dithiothreitol reductant to achieve a reduced state. However, due to restricted access to the cysteine residues, confirming their reduction with 5,5′-dithiobis (2-nitro)benzoate proved unfeasible. As a result, we were unable to assess the thermal stability of the reduced wild-type form. The T_m values were 55.5 ± 0.6 °C, 51.5 ± 0.4 °C and 48.7 ± 0.1 °C for wild-type AmGSTD1, AmGSTD1^M126L and AmGSTD1^C127S, respectively. The mutation of Cys127 to a serine and thus the disruption of the disulfide bridge would lead to a loss in thermal stability of 6.8 °C, while the mutation of Met126 to Leu would lead to a loss of 4.0 °C. These results show the importance of both residues Met126 and Cys127 for maintaining the good stability of AmGSTD1.

In conclusion, the biochemical and structural characterization of AmGSTD1 reveals original features for the sole member of this class in the honey bee. The efficient activity rate of AmGSTD1 is compatible with a fast metabolization of odorant molecules, which is indispensable for liberating the olfactory receptor and facilitating renewed detection. From an evolutionary point of view, our results suggest that keeping only one member of GST Delta could be a disadvantage to metabolize exogenous molecules, but this could have been compensated by good kinetics, as well as an enhanced stability thanks to a unique structural feature, the sulfur sandwich.

Acknowledgements

Author contributions

FN and MS conceived and supervised the study. MS, VB, MM, PF, PS, AN, FC, FL, RL, MM, TC, EA, CD and FN performed the experiments and analysed the data; FN and MS wrote the manuscript.

Peer review

The peer review history for this article is available at https://www.webofscience.com/api/gateway/wos/peer-review/10.1002/1873-3468.14770.

Data accessibility

The structural data that support the findings of this study are openly available in the wwPDB at https://doi.org/10.2210/pdb8Q89/pdb, https://doi.org/10.2210/pdb8Q8A/pdb, https://doi.org/10.2210/pdb8Q8B/pdb.

References

1 Wright GA, Nicolson SW and Shafir S (2018) Nutritional physiology and ecology of honey bees. *Annu Rev Entomol* **63**, 327–344.

2 Di Noi A, Casini S, Campani T, Cai G and Caliani I (2021) Review on sublethal effects of environmental contaminants in honey bees (*Apis mellifera*), knowledge gaps and future perspectives. *Int J Environ Res Public Health* **18**, 1863.

3 Slessor KN, Winston ML and Le Conte Y (2005) Pheromone communication in the honeybee (*Apis mellifera* L.). *J Chem Ecol* **31**, 2731–2745.

4 Schwartz M, Boichot V, Fraichard S, Muradova M, Senet P, Nicolai A, Lirussi F, Bas M, Canon F, Heydel JM *et al.* (2023) Role of insect and mammal glutathione transferases in chemoperception. *Biomolecules* **13**, 322.

5 Fang Y, Song F, Zhang L, Aleku DW, Han B, Feng M and Li J (2012) Differential antennal proteome comparison of adult honeybee drone, worker and queen (*Apis mellifera* L.). *J Proteomics* **75**, 756–773.

6 Nie H, Xu S, Xie C, Geng H, Zhao Y, Li J, Huang WF, Lin Y, Li Z and Su S (2018) Comparative transcriptome analysis of *Apis mellifera* antennae of workers performing different tasks. *Mol Genet Genomics* **293**, 237–248.

7 Fraichard S, Legendre A, Lucas P, Chauvel I, Faure P, Neiers F, Artur Y, Briand L, Ferveur JF and Heydel JM (2020) Modulation of sex pheromone discrimination by a UDP-glycosyltransferase in *Drosophila melanogaster*. *Genes (Basel)* **11**, 237.

8 Mannervik B (2012) Five decades with glutathione and the GSTome. *J Biol Chem* **287**, 6072–6083.

9 Mannervik B, Board PG, Hayes JD, Listowsky I and Pearson WR (2005) Nomenclature for mammalian soluble glutathione transferases. *Methods Enzymol* **401**, 1–8.

10 Shi H, Pei L, Gu S, Zhu S, Wang Y, Zhang Y and Li B (2012) Glutathione S-transferase (GST) genes in the red flour beetle, *Tribolium castaneum*, and comparative analysis with five additional insects. *Genomics* **100**, 327–335.

11 Roncalli V, Cieslak MC, Passamaneck Y, Christie AE and Lenz PH (2015) Glutathione S-transferase (GST) gene diversity in the crustacean *Calanus finmarchicus* – contributors to cellular detoxification. *PLoS One* **10**, e0123322.

12 Habig WH, Pabst MJ and Jakoby WB (1974) Glutathione S-transferases. The first enzymatic step in mercapturic acid formation. *J Biol Chem* **249**, 7130–7139.

13 Clark AG and Shamaan NA (1984) Evidence that DDT-dehydrochlorinase from the house fly is a glutathione S-transferase. *Pest Biochem Physiol* **22**, 249–261.

14 Hurst R, Bao Y, Jemth P, Mannervik B and Williamson G (1998) Phospholipid hydroperoxide glutathione peroxidase activity of human glutathione transferases. *Biochem J* **332** (Pt 1), 97–100.

15 Škerlová J, Lindström H, Gonis E, Sjödin B, Neiers F, Stenmark P and Mannervik B (2019) Structure and steroid isomerase activity of Drosophila glutathione transferase E14 essential for ecdysteroid biosynthesis. *FEBS Lett* **594**, 1187–1195.

16 Chanut-Delalande H, Hashimoto Y, Pelissier-Monier A, Spokony R, Dib A, Kondo T, Bohère J, Niimi K, Latapie Y, Inagaki S *et al.* (2014) Pri peptides are

mediators of ecdysone for the temporal control of development. *Nat Cell Biol* **16**, 1035–1044.

17 Enya S, Ameku T, Igarashi F, Iga M, Kataoka H, Shinoda T and Niwa R (2014) A Halloween gene noppera-bo encodes a glutathione S-transferase essential for ecdysteroid biosynthesis via regulating the behaviour of cholesterol in Drosophila. *Sci Rep* **4**, 6586.

18 Gonis E, Fraichard S, Chertemps T, Hecker A, Schwartz M, Canon F and Neiers F (2022) Expression patterns of *Drosophila melanogaster* glutathione transferases. *Insects* **13**, 612.

19 Younus F, Chertemps T, Pearce SL, Pandey G, Bozzolan F, Coppin CW, Russell RJ, Maïbèche-Coisne M and Oakeshott JG (2014) Identification of candidate odorant degrading gene/enzyme systems in the antennal transcriptome of *Drosophila melanogaster*. *Insect Biochem Mol Biol* **53**, 30–43.

20 Corcoran JA, Jordan MD, Thrimawithana AH, Crowhurst RN and Newcomb RD (2015) The peripheral olfactory repertoire of the lightbrown apple moth, *Epiphyas postvittana*. *PLoS One* **10**, e0128596.

21 Huang XL, Fan DS, Liu L and Feng JN (2017) Identification and characterization of glutathione S-transferase genes in the antennae of codling moth (Lepidoptera: Tortricidae). *Ann Entomol Soc Am* **110**, 409–416.

22 Leal WS, Ishida Y, Pelletier J, Xu W, Rayo J, Xu X and Ames JB (2009) Olfactory proteins mediating chemical communication in the navel orangeworm moth, *Amyelois transitella*. *PLoS One* **4**, e7235.

23 Liu S, Gong ZJ, Rao XJ, Li MY and Li SG (2015) Identification of putative carboxylesterase and glutathione S-transferase genes from the antennae of the *Chilo suppressalis* (Lepidoptera: Pyralidae). *J Insect Sci* **15**, 103.

24 Liu S, Zhang YX, Wang WL, Zhang BX and Li SG (2017) Identification and characterisation of seventeen glutathione S-transferase genes from the cabbage white butterfly *Pieris rapae*. *Pestic Biochem Physiol* **143**, 102–110.

25 Tan X, Hu XM, Zhong XW, Chen QM, Xia QY and Zhao P (2014) Antenna-specific glutathione S-transferase in male silkmoth *Bombyx mori*. *Int J Mol Sci* **15**, 7429–7443.

26 Wang GR, Guo YY and Wu KM (2002) Cloning of a cDNA fragment of an antenna-specific gene in *Helicoverpa armigera*. *Chin J Agric Biotechnol* **1**, 37–43.

27 Durand N, Pottier MA, Siaussat D, Bozzolan F, Maibeche M and Chertemps T (2018) Glutathione-S-transferases in the olfactory organ of the noctuid moth *Spodoptera littoralis*, diversity and conservation of chemosensory clades. *Front Physiol* **9**, 1283.

28 Rogers ME, Jani MK and Vogt RG (1999) An olfactory-specific glutathione-S-transferase in the sphinx moth *Manduca sexta*. *J Exp Biol* **202**, 1625–1637.

29 Gu XC, Zhang YN, Kang K, Dong SL and Zhang LW (2015) Antennal transcriptome analysis of odorant reception genes in the red turpentine beetle (RTB), *Dendroctonus valens*. *PLoS One* **10**, e0125159.

30 Mamidala P, Wijeratne AJ, Wijeratne S, Poland T, Qazi SS, Doucet D, Cusson M, Beliveau C and Mittapalli O (2013) Identification of odor-processing genes in the emerald ash borer, *Agrilus planipennis*. *PLoS One* **8**, e56555.

31 Ortelli F, Rossiter LC, Vontas J, Ranson H and Hemingway J (2003) Heterologous expression of four glutathione transferase genes genetically linked to a major insecticide-resistance locus from the malaria vector *Anopheles gambiae*. *Biochem J* **373**, 957–963.

32 Yamamoto K, Higashiura A, Hirowatari A, Yamada N, Tsubota T, Sezutsu H and Nakagawa A (2018) Characterisation of a diazinon-metabolising glutathione S-transferase in the silkworm *Bombyx mori* by X-ray crystallography and genome editing analysis. *Sci Rep* **8**, 16835.

33 Yamamoto K, Ichinose H, Aso Y, Banno Y, Kimura M and Nakashima T (2011) Molecular characterization of an insecticide-induced novel glutathione transferase in silkworm. *Biochim Biophys Acta* **1810**, 420–426.

34 You Y, Xie M, Ren N, Cheng X, Li J, Ma X, Zou M, Vasseur L, Gurr GM and You M (2015) Characterization and expression profiling of glutathione S-transferases in the diamondback moth, *Plutella xylostella* (L.). *BMC Genomics* **16**, 152.

35 Gonzalez D, Fraichard S, Grassein P, Delarue P, Senet P, Nicolaï A, Chavanne E, Mucher E, Artur Y, Ferveur JF *et al*. (2018) Characterization of a Drosophila glutathione transferase involved in isothiocyanate detoxification. *Insect Biochem Mol Biol* **95**, 33–43.

36 Hayes JD and Strange RC (2000) Glutathione S-transferase polymorphisms and their biological consequences. *Pharmacology* **61**, 154–166.

37 Li GW, Chen XL, Xu XL and Wu JX (2018) Degradation of sex pheromone and plant volatile components by an antennal glutathione S-transferase in the oriental fruit moth, *Grapholita molesta* Busck (Lepidoptera: Tortricidae). *Arch Insect Biochem Physiol* **99**, e21512.

38 Wongsantichon J and Ketterman AJ (2006) An intersubunit lock-and-key 'clasp' motif in the dimer interface of Delta class glutathione transferase. *Biochem J* **394**, 135–144.

39 Wongsantichon J, Robinson RC and Ketterman AJ (2015) Epsilon glutathione transferases possess a unique class-conserved subunit interface motif that directly interacts with glutathione in the active site. *Biosci Rep* **35**, e00272.

40 Claudianos C, Ranson H, Johnson RM, Biswas S, Schuler MA, Berenbaum MR, Feyereisen R and Oakeshott JG (2006) A deficit of detoxification

enzymes: pesticide sensitivity and environmental response in the honeybee. *Insect Mol Biol* **15**, 615–636.

41 Jain R and Brockmann A (2020) Sex-specific molecular specialization and activity rhythm-dependent gene expression in honey bee antennae. *J Exp Biol* **223**, jeb217406.

42 Arena M and Sgolastra F (2014) A meta-analysis comparing the sensitivity of bees to pesticides. *Ecotoxicology* **23**, 324–334.

43 Schwartz M, Brignot H, Feron G, Hummel T, Zhu Y, von Koskull D, Heydel JM, Lirussi F, Canon F and Neiers F (2022) Role of human salivary enzymes in bitter taste perception. *Food Chem* **386**, 132798.

44 Schwartz M, Menetrier F, Heydel JM, Chavanne E, Faure P, Labrousse M, Lirussi F, Canon F, Mannervik B, Briand L *et al.* (2020) Interactions between odorants and glutathione transferases in the human olfactory cleft. *Chem Senses* **45**, 645–654.

45 Niklasson M, Andresen C, Helander S, Roth MG, Zimdahl Kahlin A, Lindqvist Appell M, Martensson LG and Lundstrom P (2015) Robust and convenient analysis of protein thermal and chemical stability. *Protein Sci* **24**, 2055–2062.

46 Kabsch W (2010) XDS. *Acta Crystallogr D Biol Crystallogr* **66**, 125–132.

47 Winn MD, Ballard CC, Cowtan KD, Dodson EJ, Emsley P, Evans PR, Keegan RM, Krissinel EB, Leslie AGW, McCoy A *et al.* (2011) Overview of the CCP4 suite and current developments. *Acta Crystallogr D Biol Crystallogr* **67**, 235–242.

48 Yamamoto K, Higashiura A, Hossain MT, Yamada N, Shiotsuki T and Nakagawa A (2015) Structural characterization of the catalytic site of a *Nilaparvata lugens* delta-class glutathione transferase. *Arch Biochem Biophys* **566**, 36–42.

49 Long F, Vagin AA, Young P and Murshudov GN (2008) BALBES: a molecular-replacement pipeline. *Acta Crystallogr D Biol Crystallogr* **64**, 125–132.

50 Emsley P and Cowtan K (2004) Coot: model-building tools for molecular graphics. *Acta Crystallogr D Biol Crystallogr* **60**, 2126–2132.

51 Adams PD, Afonine PV, Bunkóczi G, Chen VB, Davis IW, Echols N, Headd JJ, Hung LW, Kapral GJ, Grosse-Kunstleve RW *et al.* (2010) PHENIX: a comprehensive Python-based system for macromolecular structure solution. *Acta Crystallogr D Biol Crystallogr* **66**, 213–221.

52 Chen VB, Arendall WB III, Headd JJ, Keedy DA, Immormino RM, Kapral GJ, Murray LW, Richardson JS and Richardson DC (2010) MolProbity: all-atom structure validation for macromolecular crystallography. *Acta Crystallogr D Biol Crystallogr* **66**, 12–21.

53 Johnson ER, Keinan S, Mori-Sanchez P, Contreras-Garcia J, Cohen AJ and Yang W (2010) Revealing

noncovalent interactions. *J Am Chem Soc* **132**, 6498–6506.

54 Lu T and Chen F (2012) Multiwfn: a multifunctional wavefunction analyzer. *J Comput Chem* **33**, 580–592.

55 Dhaka A, Jeon IR, Jeannin O, Aubert E, Espinosa E and Fourmigue M (2022) Topochemical polymerization of a diacetylene in a chalcogen-bonded (ChB) assembly. *Angew Chem Int Ed Engl* **61**, e202116650.

56 Saisawang C, Wongsantichon J and Ketterman AJ (2012) A preliminary characterization of the cytosolic glutathione transferase proteome from *Drosophila melanogaster*. *Biochem J* **442**, 181–190.

57 Sawicki R, Singh SP, Mondal AK, Benes H and Zimniak P (2003) Cloning, expression and biochemical characterization of one epsilon-class (GST-3) and ten delta-class (GST-1) glutathione S-transferases from *Drosophila melanogaster*, and identification of additional nine members of the epsilon class. *Biochem J* **370**, 661–669.

58 Bocedi A, Fabrini R, Lo Bello M, Caccuri AM, Federici G, Mannervik B, Cornish-Bowden A and Ricci G (2016) Evolution of negative cooperativity in glutathione transferase enabled preservation of enzyme function. *J Biol Chem* **291**, 26739–26749.

59 Liu H, Tang Y, Wang Q, Shi H, Yin J and Li C (2021) Identification and characterization of an antennae-specific glutathione S-transferase from the Indian meal moth. *Front Physiol* **12**, 727619.

60 Xia D, Zheng R, Huang J, Lu S and Tang Q (2022) Identification and functional analysis of glutathione S-transferases from *Sitophilus zeamais* in olfactory organ. *Insects* **13**, 259.

61 Liu JN, Xi JH, Wang Z, Zhao SW, Wang X, Bu YW, Zhou KX, Pan Y and Wang S (2023) Glutathione S-transferase highly expressed in *Holotrichia parallela* antennae inactivates the odorant unsaturated aldehyde volatiles. *J Agric Food Chem* **71**, 8797–8807.

62 Velankar S, Best C, Beuth B, Boutselakis CH, Cobley N, Sousa da Silva AW, Dimitropoulos D, Golovin A, Hirshberg M, John M *et al.* (2010) PDBe: protein data bank in Europe. *Nucleic Acids Res* **38**, D308–D317.

63 Krissinel E and Henrick K (2007) Inference of macromolecular assemblies from crystalline state. *J Mol Biol* **372**, 774–797.

64 Shukla R, Dhaka A, Aubert E, Vijayakumar-Syamala V, Jeannin O, Fourmigué M and Espinosa E (2020) Understanding reactivity and assembly of dichalcogenides: structural, electrostatic potential, and topological analyses of 3H-1,2-benzodithiol-3-one and selenium analogs. *Cryst Growth des* **20**, 7704–7725.

65 Jena S, Dutta J, Tulsiyan KD, Sahu AK, Choudhury SS and Biswal HS (2022) Noncovalent interactions in proteins and nucleic acids: beyond hydrogen bonding and pi-stacking. *Chem Soc Rev* **51**, 4261–4286.

Supporting information

Additional supporting information may be found online in the Supporting Information section at the end of the article.

Fig. S1. Non-Covalent interactions Index (NCI) analysis of the sulfur sandwich motif.

Fig. S2. Superimposition of AmGSTD1 monomer onto the structure of *Anopheles dirus* GST delta 4 (AdGSTD4, PDB 3F63) in complex with hexyl-glutathione.

Fig. S3. Crystal structures of mutants AmGSTD1^{M126L} and AmGSTD1^{C127S} and superimposition with the wild type structure.

Table S1. X-ray diffraction and refinement statistics.

Table S2. Ecological context of tested odors.